# DIPOLE ANTENNAS

## INTRODUCTION

Dipole antennas and their associated arrays are among the most common antennas used for communication systems and measurement of electric and magnetic fields. This article describes the basic nature of these antennas and some of their applications. Variations such as biconical and bowtie antennas, slot dipoles, folded dipoles, sleeve dipoles, and shunt-fed dipoles are also described.

## DIPOLE ANTENNAS

The simplest type of wire antenna is the dipole. A dipole antenna is most commonly a linear metallic wire or rod with a feed point at the center as shown in Fig. 1. Most often, a dipole antenna has two symmetrical radiating arms. Because of the symmetry of dipoles relative to the x–y plane containing the feed point, the resultant radiation is independent of $\phi$ (rotationally symmetric about the z-axis) and is shown in Fig. 2. The shape of the lobe(s) depends on the length of the antenna, as will be discussed in the next section. In general, however, dipole antennas are used for applications where the radiation is desired in the x–y plane of the antenna.

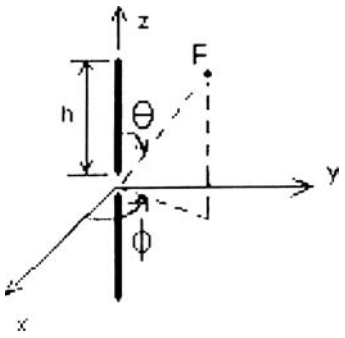


**Figure 1.** Dipole antenna.

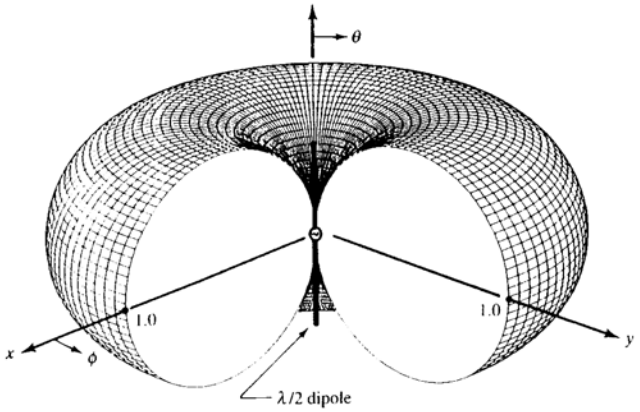


**Figure 2.** Radiation pattern for an infinitesimal (or Hertzian) dipole. (From Reference 1, © IEEE 1992.)

### Infinitesimal Dipole (Hertzian Dipole)

An infinitesimal dipole (Length L << wavelength $\lambda$) is a linear element that is assumed to be short enough that the current ($I$) is constant along its length. This element is also called a Hertzian dipole. The electric and magnetic field components of the Hertzian dipole are (2)

$$\overline{H} = \frac{1}{4\pi} IL\sin\theta\left(\frac{jk_o}{r} + \frac{1}{r^2}\right)e^{-jk_o r}\hat{\phi} \tag{1}$$

$$\overline{E} = \frac{j\eta_o IL}{2\pi k_o}\cos\theta\left(\frac{jk_o}{r^2} + \frac{1}{r^3}\right)e^{-jk_o r}\hat{r} - \frac{j\eta_o IL}{4\pi k_o}\sin\theta\left(-\frac{k_o^2}{r} + \frac{jk_o}{r^2} + \frac{1}{r^3}\right)e^{-jk_o r}\hat{\theta} \tag{2}$$

where $\eta_o = (\mu_o/\varepsilon_o)^{1/2}$ is the intrinsic impedance ($= 377\,\Omega$) for free space and $k_o = \omega(\mu_o\varepsilon_o)^{1/2}$ is the propagation constant ($= \omega/c$, where $c$ is the velocity of light). The fields are observed to decay rapidly ($1/r^3$ variation, where $r$ is the distance from the antenna, very near the antenna, and less rapidly ($1/r$ variation) farther away. The fields with terms $1/r^2$ and $1/r^3$ (the *induction terms*) provide energy that is stored near the antenna. This energy can be used for applications where heat is desired near the antenna such as for cardiac ablation or hyperthermia. The fields with $1/r$ variation (the *radiation terms*) provide energy propagation away from the antenna. These fields are used for communication applications. The distance away from the antenna where the induction and radiation terms are equal is $r = \lambda/2\pi$. When $r < \lambda/2\pi$, this is the *near field* of the antenna, and the induction terms dominate. When $r > \lambda/2\pi$, this is the *far field*, and the radiation terms dominate. In the far field, the wave propagation is in the transverse electromagnetic (TEM) mode, which is characteristic of far-field radiation from finite structures.

The far-zone radiated fields of the Hertzian dipole follow from equations (1) and (2) by retaining the $1/r$ varying terms:

$$\overline{H} = \frac{j}{4\pi r} IL\sin\theta e^{-jk_o r}\hat{\phi} \tag{3}$$

$$\overline{E} = \frac{j\eta_o}{4\pi r} IL\sin\theta e^{-jk_o r}\hat{\theta} \tag{4}$$

As expected for TEM wave propagation, the **E** and **H** fields are perpendicular to each other and to the outward propagation in the **r** direction. Also the ratio of $\mathbf{E}/\mathbf{H} = \eta_o = (\mu_o/\varepsilon_o)^{1/2}$, which is the intrinsic impedance of free space.

The radiation pattern of the Hertzian dipole is shown in Fig. 2 and exhibits the classic symmetry expected of dipole antennas, being both independent of $\phi$ and symmetric about the x–y plane through the center (feed point) of the dipole. The magnitude of the total radiated power is $P_{\text{rad}} = 40\,\pi^2 I_o^2 (L/\lambda)^2$, where $I_o$ is the current on the dipole. From equations 3 and 4, it is interesting to note that, even for this constant-current infinitesimal dipole, the radiated power density is proportional to $\sin^2\theta$. Hence, it is maximum for $\theta = 90^\circ$ (i.e., in the x–y plane normal to the orientation of the dipole) and zero for the directions along the length of the dipole ($\theta = 0^\circ$ and $180^\circ$). The latter property for zero radiation along the length of the dipole is observed for all linear antennas regardless of length, which follows from the fact that a linear antenna of finite length may be

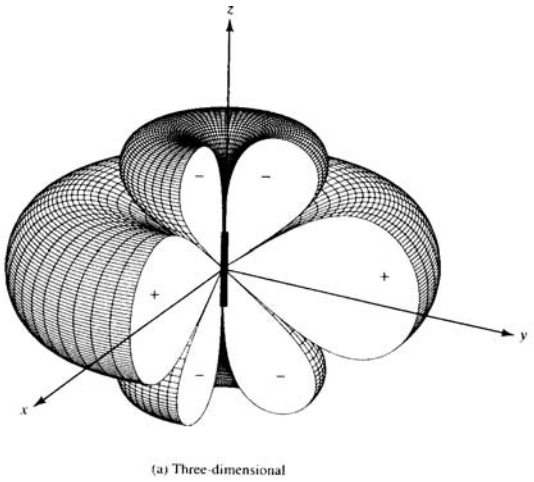


**Figure 3.** (a) Current distributions. (From Reference 3.) (b) Radiation patterns for a 1.25 λ dipole antenna.

considered to be composed of a set of infinitesimal dipoles. As the infinitesimal dipoles do not create **E** and **H** fields or radiated power density for the $\theta = 0^\circ$ and $180^\circ$ directions, the sum of many of them also does not have power in these directions.

### Linear Dipole Antennas

The geometry of a linear dipole antenna of length-2h is shown in Fig. 1. The current distribution is sinusoidal and is given by

$$I(z) = \frac{I(0)}{\sin kh}\sin k(h - |z|) \; for - h < z < h \tag{5}$$

where $I(0)$ is the current at the feed point of the antenna, $h$ is the half length of the antenna, and $k = \omega(\mu\varepsilon)^{1/2}$ is the propagation constant in the material surrounding the dipole. The current distributions for several lengths of dipole antennas are shown in Fig. 3.

The electric and magnetic fields around the dipole are calculated by modeling the antenna as a series of Hertzian dipoles having different current strengths shown by the patterns in Fig. 1 and by integrating the fields from each of these elements. The resultant fields far from the antenna at a distance $r$ are

$$\overline{E} = \frac{j\eta I(0)}{2\pi r_o \sin(kh)} F(\theta) e^{j(\omega t - kr_o)}\hat{\theta} \tag{6}$$

and

$$\overline{H} = \frac{jI(0)}{2\pi r_o \sin(kh)} F(\theta) e^{j(\omega t - kr_o)}\hat{\phi} \tag{7}$$

where $\eta = (\mu\varepsilon)^{1/2}$, and the $\theta$-dependence of the radiated fields $F(\theta)$ is called the pattern factor and is given by the following:

$$F(\theta) = \frac{\cos(kh\cos(\theta)) - \cos kh}{\sin\theta} \tag{8}$$

The radiated power density (*radiation pattern*) is given by

$$P(\theta) = \frac{\vec{E} \bullet \vec{E}^*}{2\eta}\hat{r} = \frac{\eta I^2(0)}{8\pi^2 r^2 \sin^2(kh)} F^2(\theta) \tag{9}$$

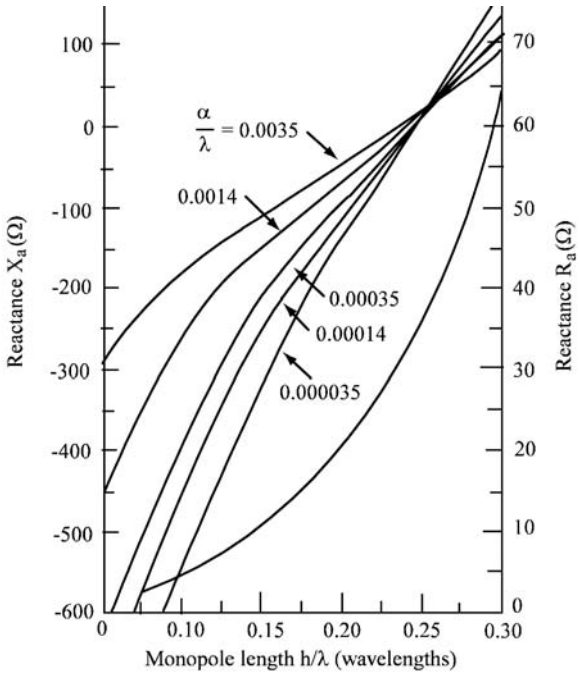


**Figure 4.** Variation of feed-point $R_a$ and reactance $X_a$ for an end-fed monopole above ground as a function of height $h/\lambda$. Values for dipoles are double that of monopoles. (From Reference 4, p 543.)

Using $\eta = \eta_o = 120\pi$, this can also be expressed in terms of the total radiated power $W(= I^2(0)R_a/2)$ and the feed-point resistance $R_a$ as follows:

$$P(\theta) = \frac{30}{\pi r_o^2}\frac{W}{R_a}\frac{F^2(\theta)}{\sin^2 kh} \tag{10}$$

The normalized radiation patterns are shown in Fig. 3b for several different lengths of dipoles and monopoles above ground. The radiation patterns for the dipole and monopole are the same, except that the monopole does not radiate in the lower half plane and therefore radiates twice the power in the upper half plane. Mathematically, this is accounted for, because the feed-point resistance $R_a$ of the monopole is half that of the dipole, as will be discussed later in this section.

The directivity of a dipole antenna is the power density in the direction of maximum radiation (at a specified distance $r_o$) normalized by the power density of an isotropic radiator. Directivity is given by

$$D = \frac{P_{\max}}{P_o} = \frac{F^2(\theta)_{\max}}{\frac{1}{2}\int_0^\pi F^2(\theta)\sin\theta d\theta} = \frac{120}{R_a}\frac{F^2(\theta)|_{\max}}{\sin^2 kh} \tag{11}$$

where $P_o = W/(4\pi r^2)$ is the power density of an isotropic radiator.

A graph of the variation of the feed-point resistance and reactance of a monopole antenna above ground is given in Fig. 4 as a function of length $h/\lambda$, where λ is the free-space wavelength at the radiation frequency (4). Note that the reactance $X_a$ depends on the conductor radius $a$, whereas the feed-point resistance $R_a$ is relatively independent of conductor radius $a$ for thin antennas ($a/\lambda \leq 1$). The input

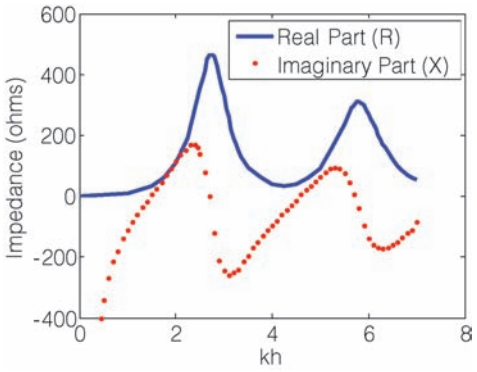


**Figure 5.** Input Impedance of a cylindrical dipole antenna with h/a = 60. From [E. Hallen, Admittance Diagrams for Antennas and the Relation between Antenna Theories, Cruft Laboratory, Harvard University, Technical Report 46, June 1948].

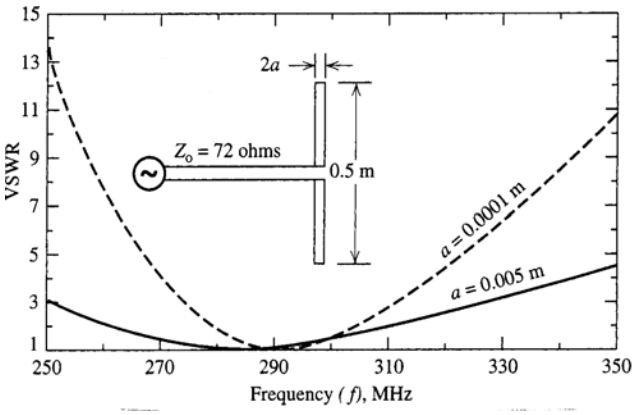


**Figure 6.** VSWR of a dipole antenna as a function of frequency and wire thickness. (From Reference 6.)

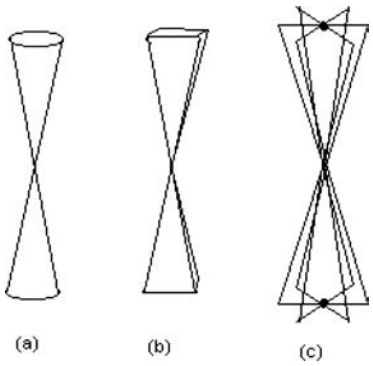


**Figure 7.** Biconical dipole antenna and variations: (a) biconical dipole antenna, (b) flat bow-tie antenna, and (c) wire version of biconical dipole antenna.

resistance $R_a$ of a center-fed dipole antenna of length $2h$ is twice that of an end-fed monopole of length $h$.

The ohmic losses of a dipole antenna (given by $I^2(0)$ $R_{\text{ohmic}}/2$) are small, particularly for $h/\lambda > 0.1$. The resultant antenna radiation efficiencies [given by $R_a/(R_a + R_{\text{ohmic}})$] are on the order of 90–99%.

Physical dipoles act slightly differently than predicted, because they have some finite thickness, and the ends of the wire capacitively couple to air. This effectively makes the antenna electrically longer than its physical length by 2% to 9%. For a half-wave dipole (length $= 2h = \lambda/2$), for instance, the physical length must be slightly shortened to create a resonant length antenna ($X_a = 0$). Table 1 shows the wire lengths required to produce a resonant half-wave dipole. This shortening factor varies from 2% to 9%, depending on the thickness of the dipole.

As a dipole antenna is a physically resonant structure, its feed-point impedance (particularly the reactance $X_a$) varies greatly with frequency. The input impedance of a dipole antenna is shown in Fig. 5. Thus, these antennas have a fairly narrow bandwidth. The VSWR of a dipole antenna as a function of frequency and wire thickness is shown in Fig. 6 for an antenna that would be half-wave resonant at 300 MHz. Using a measure of "useable bandwidth" that the measured VSWR should be less than 2:1, this antenna has bandwidths of 310−262 = 48 MHz for the thicker wire and 304−280 = 24 MHz for the thinner wire. As fractions of the design frequency (300 MHz), the bandwidths are 16% and 8%, respectively.

## Specialized Dipole Antennas

**Slot Dipole.** A slot dipole antenna is a dual to the linear dipole antenna. A slot antenna is produced by creating a thin slot of length $h$ in a conducting metal sheet and by feeding it in the center of the slot. The radiation pattern of a slot antenna is identical to that of the linear dipole of the same length (see Fig. 3) except that orientations of the **E** and **H** are interchanged, which means that the power pattern is the same, even though the orientation of the fields is different. Also the feed-point impedance $Z_s$ of a slot antenna is related to that of the dual linear antenna by the following equation:

$$Z_s = \frac{\eta^2}{4Z_a} \tag{12}$$

where $Z_s$ is the impedance of the slot and $Z_a$ is the impedance of the dual linear antenna. Cavity-backed slot antennas with integrated matching networks are among the smallest (physical size/electrical size) antennas available (7).

**Biconical Dipoles.** A biconical dipole, such as shown in Fig. 7a, is commonly used for broadband applications. Typical flare angles $\theta$ are between 30° and 60°. The exact flare angle is not critical, so it is generally chosen so that the impedance of the dipole nearly matches the impedance of the feed line to which it is connected. The impedance of the biconical dipole varies as a function of wavelength and flare angle, with a relatively flat impedance response for wide flare angles. Hence, this antenna is broader band than a simple linear dipole. Some variations of this method of using flaring to increase bandwidth are the flat bow-tie antenna (which may be built on a printed circuit board) and the wire version of the biconical antenna shown in Fig. 7b and c, respectively.

**Folded Dipole Antennas.** A folded dipole antenna is shown in Fig. 8. The dipole is created by joining two cylin-

Table 1. Wire Lengths Required to Produce a Resonant Half-Wave Dipole for a Wire Diameter of 2a and a Length L

| Length-to-diameter ratio, L / (2a) | Percent shortening required | Resonant length | Dipole thickness class |
|---|---|---|---|
| 5000 | 2 | 0.49 λ | Very thin |
| 50 | 5 | 0.475 λ | Thin |
| 10 | 9 | 0.455 λ | Thick |

Table 2. Relationships Between Monopole and Dipole Antennas

| | Monopole above ground-length = $h$ | Corresponding dipole of twice length $L = 2h$ |
|---|---|---|
| Radiation pattern | Same as that for the dipole but only for angle $0 \le \theta \le 90^\circ$ | |
| Feed-point reactance $R_a$ | $R_a mono\ pole\| = \frac{1}{2} R_{a,d}(2h)$ | $R_{a,d}$ : function of length$L = 2h$ (see Fig. 2) |
| Feed-point reactance $X_a$ | $X_a mono\ pole\| = \frac{1}{2} X_{a,d}(2h)$ | $X_{a,d}$ : function of length$L = 2h$ (see Fig. 2) |
| Directivity $D_a$ | $D_a mono\ pole\| = \frac{1}{2} 2D_{a,d}(2h)$ | $D_{a,d}$ : function of length$L = 2h$ |

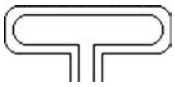

**Figure 8.** Folded dipole antenna.

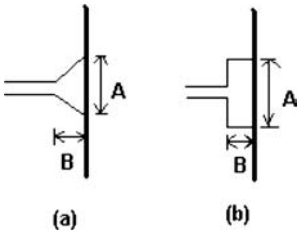


**Figure 9.** Shunt-fed dipoles: (a) delta match and (b) T-match.

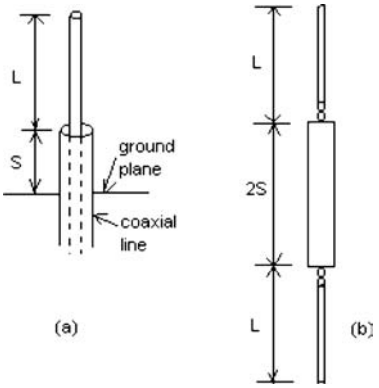


**Figure 10.** Sleeve dipole antenna: (a) physical model and (b) equivalent electrical model.

drical dipoles at the ends and driving the entire structure by a transmission line (often a two-wire transmission line) at the center of one arm as shown. The feed-point impedance of a folded dipole of two identical-diameter arms is four times as large as for an unfolded dipole of the same length, which can actually be advantageous, because the feed-point resistance may now be comparable with the characteristic impedance $Z_o$ of the transmission or feed line. The reactance of the antenna may easily be compensated by using a lumped element with a reactance that is negative of the reactance at the terminals of the folded dipole antenna or else by using a foreshortened antenna length to resonant length arms so that $X_a = 0$ (see Table 1).

**Shunt-Fed Dipoles.** Matching networks of reactive elements are generally required to match the feed-point impedance ($R_a + j X_a$) of center-fed dipoles to transmission lines. Typically these lines have characteristic impedance on the order of 300 Ω to 600 Ω, and a thin half wave dipole has impedance $Z = 73 + j\ 42$ Ω. To alleviate the need for matching networks, the dipoles are at times shunt-fed at symmetric locations off the center point as shown in Fig. 9. This procedure using either the delta match (Fig. 9a) or the T-match (Fig. 9b) is often used for half-wave dipoles ($2h = \lambda/2$) with A and B dimensions that are typically on the order of 0.10 to 0.15 λ.

**Sleeve Dipole.** The sleeve dipole antenna and its equivalent electrical model are shown in Fig. 10. In practice, this antenna is built from a coaxial line with the outside conductor and insulation stripped away from the center conductor, which is left protruding. The outer conductor is connected to the ground plane, and the image produced by the ground plane creates an equivalent sleeve dipole antenna. These dipoles are useful, because they have a broad band VSWR over nearly an octave of bandwidth.

## Dipole Antenna Arrays

Dipole antennas and arrays of dipole antennas are used for short wave (3 MHz to 30 MHz) and for VHF and UHF (30 MHz to 900 MHz) radio and TV broadcasting. If directional communication is desired such as for short-wave radio transmission via the ionosphere, a phased array of horizontal dipoles may be used mounted above a ground plane. The spacing is chosen to send the major lobe of radiation toward the sky at a suitable angle to reflect off the ionosphere and to provide broadcast coverage over the desired service area.

For VHF and UHF radio and TV broadcasting over a 360° azimuthal angle, colinearly mounted vertical dipoles that are excited in-phase with each other are often used. Two examples of this are shown in Fig. 11a and b. An example variation of this is a three- to eight-bay turnstile

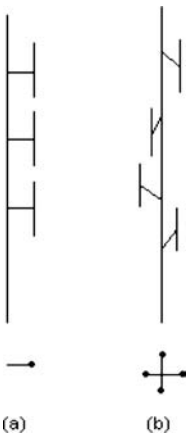


**Figure 11.** Colinearly mounted vertical dipoles for VHF and UHF radio and TV broadcasting: (a) pole-mounted array of colinear dipoles and (b) vertical dipoles spaced around a pole.

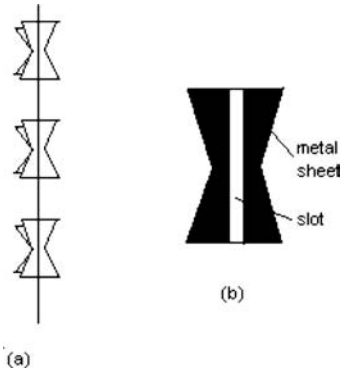


**Figure 12.** Variation on colinearly mounted vertical dipoles: (a) turnstile antenna used for TV broadcasting and (b) one of two perpendicular slot antennas that comprise each turnstile.

antenna used for TV broadcasting shown in Fig. 12a. Each turnstile is made of two perpendicular slot antennas as shown in Fig. 12b.

**Log-Periodic Antennas.** For broadband applications, log-periodic antennas are commonly used as both transmitting and receiving antennas. The bandwidth is easily controlled by adjusting the relative lengths of the longest and shortest elements in the array. The geometry of a log-periodic array is shown in Fig. 13a, which shows how the "phase-reversal" feed system for this antenna is constructed. The equivalent antenna model of this array is shown in Fig. 13b. The elements of the array are dipole antennas that increase in both length and spacing according to the formula:

where $\tau = f_n / f_{n+1}$ is the ratio of the resonant frequencies $f_n$ and $f_{n+1}$ of the adjacent dipole

$$\tau = \frac{R_{n+1}}{R_n} = \frac{d_{n+1}}{d_n} \tag{13}$$

elements. As lengths and spacings are interrelated, the choice of one initial value controls the design of the remaining elements. The spacing between one half-wave dipole

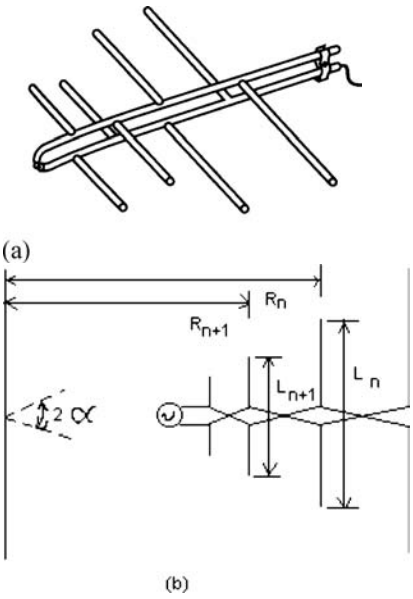


**Figure 13.** Log-periodic dipole array: (a) geometry of a log-periodic array showing how the "phase-reversal" feed system for this antenna is constructed. (From Reference 8.) (b) Equivalent antenna model of the log-periodic array. © Mc Graw-Hill 1993.

and its adjacent shorter neighbor is given by

$$\sigma = \frac{d_n}{2L_n} = \frac{(1-\tau)}{4}\cot\alpha \tag{14}$$

Log-periodic arrays are generally constructed with small values of $\alpha$ [$10^\circ \le \alpha \le 45^\circ$ (3)] and large values of $\tau$ [$0.95^\circ \le \tau \le 0.7^\circ$ (3)] that essentially gives a traveling wave propagating to the left in the backfire direction, away from the antenna array. The nature of this array is that only the elements that are approximately a half-wavelength long radiate, and as they are radiating to the left, the smaller elements do not interfere with them. This effect is accomplished by the phase-reversal of the feeds. An array that is built without the phase-reversal radiates in the end-fire direction. The interference of the longer elements to the right of radiating elements results in spurious reflections and erratic impedance behavior, which is known as the "end effect."

An effective way to further increase the bandwidth of a log-periodic antenna is to change from dipole elements to elements with individual broader bandwidths, similar to changing from a dipole antenna to a biconical antenna. This effect is accomplished for log-periodic arrays by using a configuration of wires such as shown in Fig. 14, where each element is a sawtooth element and therefore has broader bandwidth than the individual dipole elements.

**Broadband Dipole Curtain Arrays.** A broadband dipole curtain such as shown in Fig. 15 is commonly used for high-power (100 kW to 500 kW), high-frequency ionospheric broadcasting and short-wave broadcasting stations. The curtain is composed of several dipoles, usually a half-wavelength long, mounted horizontally or vertically in a rectangular or square array, often backed by a reflecting

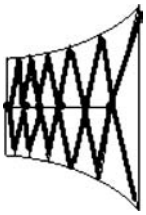

**Figure 14.** LPA with sawtooth wire elements for increased bandwidth.

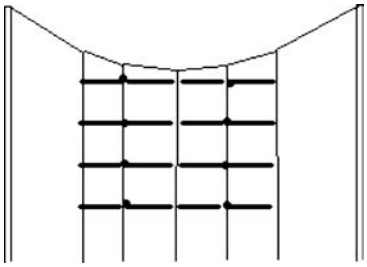

**Figure 15.** A broadband dipole curtain.

plane or wire mesh. This array has several desirable features, including high gain, broad bandwidth, independent control of horizontal and vertical radiation patterns, ease of matching (low VSWR), and the ability to efficiently broadcast efficiently. Using a phased-feed system, this array allows beam steering of the radiation pattern in both the azimuthal and the elevation planes, providing a very high degree of flexibility.

**Yagi–Uda Dipole Array.** Yagi–Uda arrays are commonly used as general-purpose antennas from 3 MHz to 3000 MHz, in particular, as home TV antennas. They are inexpensive, have reasonable bandwidth, and have gains up to 17 dBi or more if multiple arrays are used. They have unidirectional beams with moderate side lobes (8).

A typical Yagi–Uda array is shown in Fig. 16. This array is a simple end-fire array of dipole antennas where only one element is driven and the rest are parasitic. The parasitic elements operate as either reflectors or directors. In general (8), the longest antenna, which is about $\lambda/2$ in length, is the main reflector and is generally spaced $\lambda/4$ in back of the driven dipole. The feed element is commonly a folded dipole antenna 0.45 $\lambda$ to 0.49 $\lambda$ long. Adding directors, which are generally 0.4 $\lambda$ to 0.45 $\lambda$ long, to the front of the driven element increases the gain of the array. The directors are not always of the same length, diameter, or spacing. Common arrays have 6 to 12 directors and at most 2 reflectors. Additional improvements in gain by adding more elements are limited; however, arrays have been designed with 30 to 40 elements (3). A gain (relative to isotropic) of 5 to 9 per wavelength of array length is typical for Yagi–Uda arrays, for an overall gain of 50 to 54 (14.8 to 17.3 dB).

The Yagi–Uda array is characterized by a main lobe of radiation in the direction of the director elements and small side lobes. The beamwidth is small, generally 30–60° (3). Typical E and H plane patterns of a Yagi–Uda array are shown in Fig. 17. Typically, the performance of a Yagi-Uda array is computed using numerical techniques (10). For

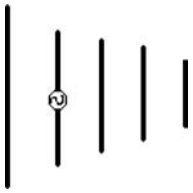

**Figure 16.** Yagi–Uda array.

the simple case where all elements are approximately the same size, the electric field pattern can be computed from the array factors of the various elements.

The input impedance of a Yagi–Uda array is often small. For example, for a 15-element array with reflector length = 0.5 $\lambda$, director spacing = 0.34 $\lambda$, and director length = 0.406 $\lambda$, the input impedance is 12, 22, 32, 50, or 62 $\Omega$ for reflector spacings of 0.10, 0.13, 0.15, 0.18, and 0.25 $\lambda$, respectively. This small inpedance can make matching to typical transmission lines (50, 75, or 300 $\Omega$) difficult. Folded dipoles used for the driven element are therefore used to boost the input impedance by a factor of four or more.

Extensive studies of the design of Yagi–Uda arrays have been made (11, 12), and tables are provided to optimize the Yagi–Uda array for a desired gain.

**Crossed Dipoles for Circular Polarization.** For applications that require a circularly polarized antenna such as TV and FM broadcasts and space communications, at least two dipoles, each of which has a linear polarization, must be combined in an array, often referred to as *crossed dipoles*. Several possible configurations are shown in Fig. 18. In a crossed dipole configuration, dipoles are mounted perpendicular to each other for circular polarization or at other angles for elliptical polarization. Currents are fed 90° out of phase between the two dipoles. These currents can also be used as probes for sensing vector fields to isolate individual components of the electric field. Adaptations of the crossed dipole are shown in ca and b. Dipole arrays such as the Yagi–Uda can also be combined to provide circular polarization, as shown in Fig. 13c.

## Modern Applications of Dipole Antennas

**Printed Dipole Antennas.** Monopoles and dipoles are not limited to wire devices. Printed monopoles (13) and dipoles (14) have also been designed and are in many cases easier to fabricate than a wire-type device. Figure 19 shows one such printed monopole used for dual-band wireless local area network coverage in the Industrial, Scientific, and Medical (ISM) bands of 2.4–2.4835 GHz and 5.15–5.825 GHz, and Figure 20 shows a printed dipole used for measurement of electric fields for evaluation of cell phone compliance with ratio-frequency (RF) exposure guidelines.

**Dipole Antennas for Medical Imaging.** Confocal imaging for breast cancer detection is an exciting application of antenna arrays in medical imaging. This method typically uses a single antenna scanned in a flat array pattern above the breast or a cylindrical array of very small broadband antennas (15). For planar imaging, the patient lies face up, and the antenna is physically scanned in a plane above the

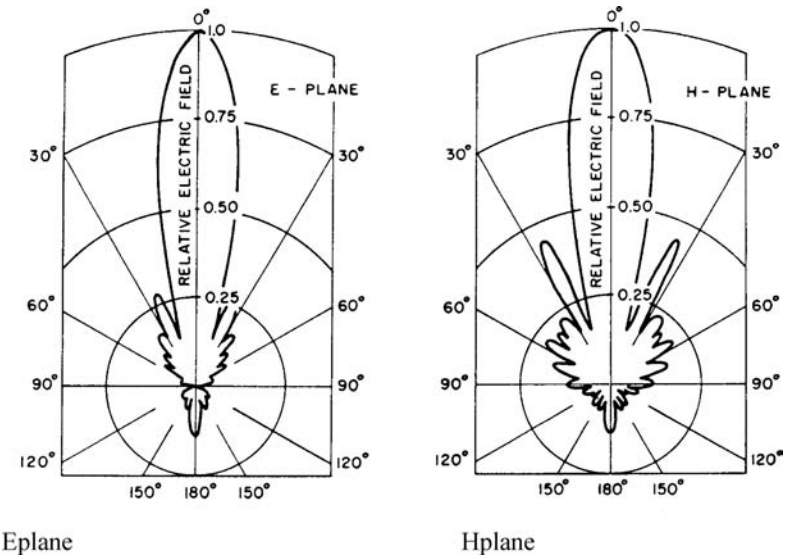


**Figure 17.** Typical E and H plane patterns of a Yagi–Uda array. Total number of elements = 27, number of directors = 25, number of reflectors = 1, number of driven elements = 1, total length of reflector = 0.5 λ, total length of feeder = 0.47 λ, total length of each director = 0.406 λ, spacing between reflector and feeder = 0.125 λ, spacing between adjacent directors = 0.34 λ, and radius of wires = 0.003 λ. (From Reference 9.) © IEEE 1969.

breast (16–18). For cylindrical imaging, the patient lies face down, with the breast extending into the cylindrical array through a hole in the table (19, 20). Matching fluid surrounding the breast, similar to that used for microwave tomography, is suggested in this case. Both methods provide similar results (20). One antenna in the array transmits an ultra-wideband (UWB) pulse, which propagates into the breast, where it is reflected off significant electrical discontinuities and is received in parallel by the other antennas in the array. Knowing the physical spacing between the array elements, the different delays among the transmit antenna, scattering point, and receiving antenna can be calculated geometrically. The received pulses representing a specific point in space can then be time delayed appropriately for each antenna, added up, and integrated to indicate the magnitude of the scattered energy from that point in space. This process is effectively correlating the signals received from that point at all antennas.

The antennas used for confocal imaging must be ultra-wideband and small enough to fit within the relatively small array area. Resolution of less than 1 cm requires a bandwidth of at least 5 GHz. The lossy nature of tissue attenuates high-frequency signals, limiting the upper frequency to about 10 GHz. Initially, resistively loaded bow-tie antennas were suggested for the planar configuration 16–18,21,22, whereas dipole antennas were suggested for the cylindrical system (19, 20). Resistively loaded Vee dipoles have also been proposed (23). In the cylindrical configuration, multiple antennas are present in the array, although they are not simultaneously active. In the planar system, a single antenna is scanned over the surface, creating a synthetic antenna aperture. To overcome the inherent inefficiency of resistively loaded antennas, a modified ridged horn antenna operating from 1 to 11 GHz has been introduced (23). Most antennas are designed to observe copolarized reflections from the breast; however, using two resistively loaded bow-tie antennas in the shape of a Maltese cross shown in Reference 24 has also been proposed to pick up the cross-polarized reflections (18). Cross-polarized reflections from simple tumor models were also examined in References 24 and 25.

The antenna shown in Figure 21 (24) consists of two cross-polarized bow-tie antenna elements, an octagonal cavity behind the bow-tie elements, and a metal flange attached to the cavity. The broadband bow-ties have flare angles of 45°. They are 1.67 cm long, which is a half-wavelength at 3 GHz in fat (similar to breast). The octagonal cavity blocks waves radiated away from the breast. The cavity is approximated as a circular waveguide filled with fat material for matching and size reduction. The first cutoff frequency is set to be 2 GHz for 2–4 GHz operation. The cavity length is a quarter-wavelength, which is 11 mm at 3 GHz. The flange consists of an inner and outer component and is designed to block unwanted waves such as surface waves. The antenna performance does not change significantly when the flange size is varied between 10 and 6.25 cm; therefore, the width of the outer flange is set to be 6.25 cm. The inner flange is designed to prevent possible electric field overshoot at the inner corners of the opening of the octagonal cavity or at the ends of the bow-tie elements. A slotline bow-tie antenna has also been proposed in Reference 26.

**Vector Antennas.** Loop antennas have received considerable attention lately in the development of compact wireless communication systems when integrated with other antennas such as dipoles. This use of loop antennas leads to the possible development of compact Multiple Input Multiple Output (MIMO) systems, which can find applications not only in communication systems, but also in the direction of arrival estimation, sensor networks, and imaging. Although, traditionally, the increase in channel capacity in

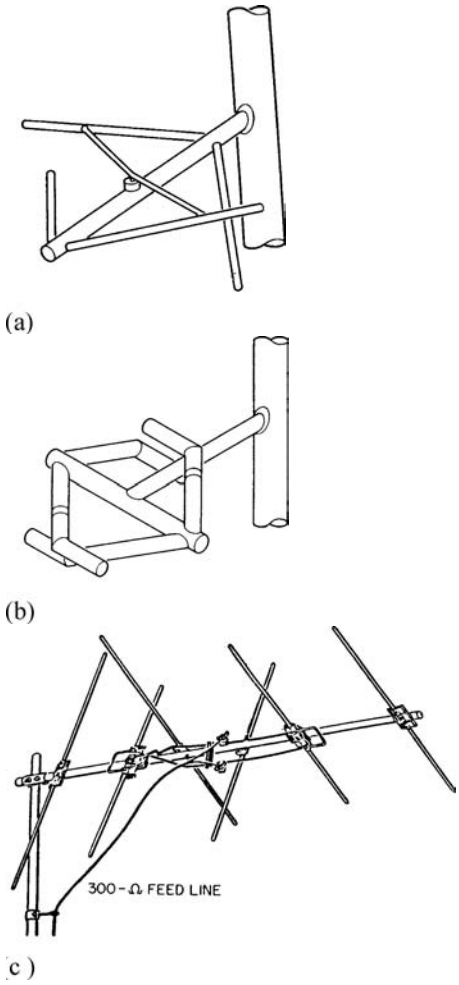


**Figure 18.** Cross-dipole applications for circular or elliptical polarization. (From Reference 8.) (a) Two shunt-fed slanted V-dipoles, (b) series-fed slanted dipoles, and (c) Circularly polarized Yagi–Uda array.

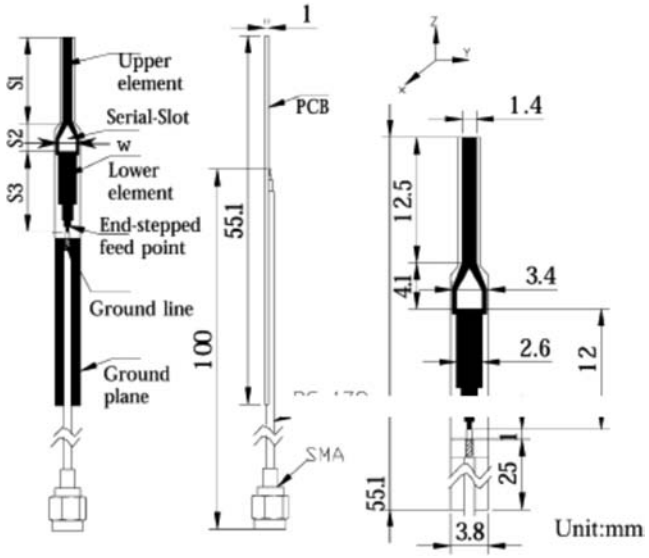


**Figure 19.** Geometry and dimensions of the proposed dual ISM-band antenna. (From Reference (13), © IEEE 2005.)

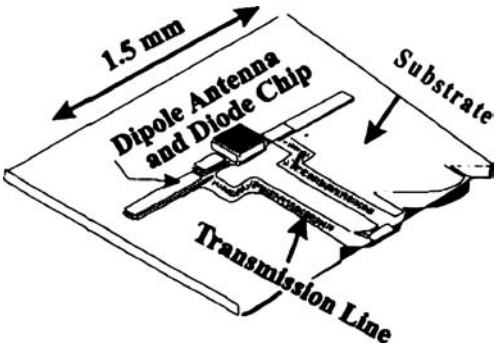


**Figure 20.** Miniature printed dipole antenna. (From Reference 14, © IEEE 1997.

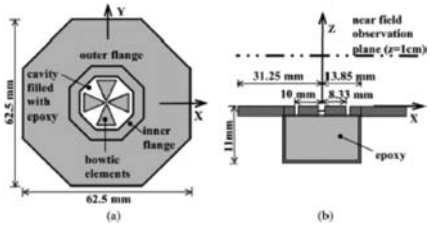


**Figure 21.** Cross-polarized antenna for confocal imaging. The properties of the substance inside the cavity and the medium outside the antenna are similar to fat ($\varepsilon_r$ = 9; $\sigma$ = 0:2 S/m). (From Reference 24.) © IEEE 2005.

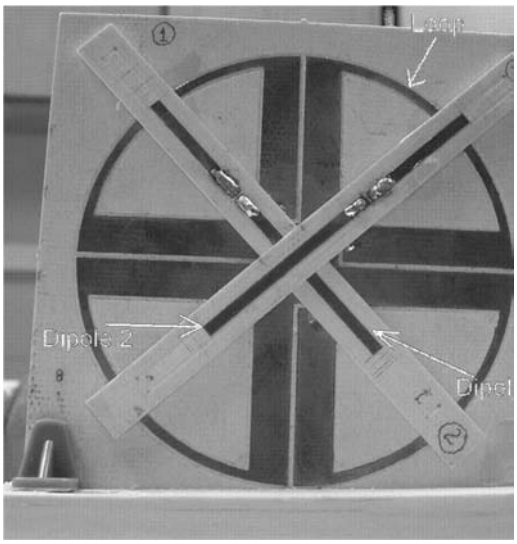


**Figure 22.** Vector antenna.

a communication system has been achieved through spatial array of antennas, similar increases in channel capacity have been obtained through the use of "vector antennas" consisting of colocated loops and dipoles, which can respond to more than one component of the electromagnetic field. One example of such antennas is given in Reference 27, where three- and four-element vector antennas, consisting of one loop and two or three dipoles, respectively, are employed in a MIMO system. Several research efforts that address the characterization of systems of colocated loops and dipoles can be found in the literature (27–32).

In Reference 27, for example, it is shown experimentally that, in a rich multipath, scattering environment systems with three- and four-element vector antennas at both the transmitter and the receiver support three and four times more information, respectively, as compared with conventional systems consisting of sensors with single antennas. Fig. 22 shows an example of a three-element vector antenna. In this particular system, as the loop must have a constant current distribution to retain the radiation characteristics of a magnetic dipole, the loop was realized by means of four pie-shaped sectors fed in phase at their corners (33). This arrangement ensured that the currents were directed in opposite directions along adjacent feed lines, thus effectively nullifying any spurious radiation. Ultra-wideband versions of such systems have also been developed for imaging purposes.

## BIBLIOGRAPHY


1. Balanis, C. A. Antenna Theory: A Review. *Proc. IEEE* 1992, **80**.
2. Johnson, R. C. *Antenna Engineering Handbook*, 3rd ed.; McGraw-Hill: New York, 1993.
3. Balanis, C. *Antenna Theory, Analysis and Design*, 3rd ed.; Wiley: New York, 2005.
4. Jordan, E. C.; Balmain, K. G. *Electromagnetic Waves and Radiating Systems*, 2nd ed.; Prentice-Hall: Englewood Cliffs, NJ, 1968.
5. Jordan, E. C.; Balmain, K. G. *Electromagnetic Waves and Radiating Systems*; Prentice Hall: Englewood Cliffs, NJ, 1968.
6. Stutzman, W. L.; Thiele, G. A. *Antenna Theory and Design*; Wiley: New York, 1991.
7. Hong, W.; Behdad, N.; Sarabandi, K. Size Reduction of Cavity-Backed Slot Antennas. *IEEE Trans. Antennas Propagat* 1996, **54**, pp 1461–1466.
8. Johnson, R. C. *Antenna Engineering Handbook*, 3rd ed.; McGraw-Hill: New York, 1993.
9. Theile, G. A. Analysis of Yagi-Uda Antennas. *IEEE Trans. Antennas Propagat.* 1969, **17**.
10. Thiele, G. A. Analysis of Yagi-Uda type antennas. *IEEE Trans. Antennas Propagat.* 1966, **14**, pp 648–649.
11. Cheng, D. K.; Chen, C. A. Optimum Spacings for Yagi-Uda Arrays. *IEEE Trans. Antennas Propagat.* 1973, **21**, pp 615–623.
12. Chen, C. A.; Cheng, D. K. Optimum Element Lengths for Yagi-Uda Arrays. *IEEE Trans. Antennas Propagat.* 1975, **23**, pp 8–15.
13. Chen, I.-F.; Peng, C.-M.; Liang, S.-C. Single Layer Printed Monopole Antenna for Dual ISM-Band Operation. *IEEE Trans. Antennas Propagat.* 2005, **53**, pp 1270–1273.
14. Bassen, H. I. Electric Field Probes for Cellular Phone Dosimetry. *Proc. 19th International Congress IEEE/EMBS Society*; Chicago, IL, Oct. 30–Nov. 2, 1997.
15. Camart, J.-C. et al.Coaxial Antenna Array for 915 MHz Interstitial Hyperthermia: Design and Modelization—Power Deposition and Heating Pattern—Phased Array. *IEEE Trans. Microw. Theory Tech.* 1992, **40**, pp 2243–2250.
16. Fear, E. C.; Hagness, S. C.; Meaney, P. M.; Okieniewski, M.; Stuchly, M. Enhancing Breast Cancer Detection using Near Field Imaging. *IEEE Microw. Mag.* 2002, pp 48–56.
17. Hagness, S. C.; Taflove, A.; Bridges, J. E. Two-Dimensional FDTD Analysis of a Pulsed Microwave Confocal System for Breast Cancer Detection: Fixed-Focus and Antenna-Array Sensors. *IEEE Trans. Biomed. Eng.* 1998, **45**, pp 1470–1479.
18. Hagness, S. C.; Taflove, A.; Bridges, J. E. Three-Dimensional FDTD Analysis of a Pulsed Microwave Confocal System for Breast Cancer Detection: Design of an Antenna-Array Element. *IEEE Trans. Antennas Propagat.* 1999, **47**, pp 783–791.
19. Li, X.; Hagness, S. C. A Confocal Microwave Imaging Algorithm for Breast Cancer Detection. *IEEE Microw. Wireless Comp. Lett.* 2001, **11**, pp 130–132.
20. Fear, E.; Stuchly, M. Microwave System for Breast Tumor Detection. *IEEE Microw. Guided Wave Lett.* 1999, **9**, pp 470–472.
21. Yun, X.; Fear, E. C.; Johnston, R. H. Compact Antenna for Radar-Based Breast Cancer Detection. *IEEE Trans. Antennas Propagat.* 2005, **53**, pp 2374–2380.
22. Hernandez-Lopez, M. A.; Pantoja, M.; Fernandez, M.; Garcia, S.; Bretones, A.; Martin, R.; Gomez, R. Design of an Ultra-Broadband V Antenna for Microwave Detection of Breast Tumors. *Microw. Opt. Tech. Lett.* 2002, **34**, pp 164–166.
23. Hagness, S. C.; Taflove, A.; Bridges, J. E. Wideband Ultralow Reverberation Antenna for Biological Sensing. *Electron, Lett.* 1997, **33**, pp 1594–1595.
24. Fear, E. C.; Stuchly, M. A. Microwave Detection of Breast Cancer. *IEEE Trans. Microwave Theory Tech.* 2000, **48**, pp 1854–1863.
25. Li, X.; Hagness, S. C.; Choi, M. K.; Choi, D. W. W. Numerical and Experimental Investigation of an Ultrawideband Ridged Pyramidal Horn Antenna with Curved Launching Plane for Pulse Radiation. *IEEE Antennas Wireless Propagat. Lett.* 2003, **2**, pp 259–262.
26. Yun, X.; Fear, E. C.; Johnston, R. H. Radar-Based Microwave Imaging for Breast Cancer Detection: Tumor Sensing with Cross-Polarized Reflections. *IEEE Antennas Propagat. Soc. Symp. Dig.* 2004, **3**, pp 2432–2435.
27. Konanur, A.; Gosalia, K.; Krishnamurthy, S.; Hughes, B.; Lazzi, G. Compact MIMO Systems Employing Vector Antennas for Increased Wireless Channel Capacity. *IEEE Trans. Microw. Theory Tech.* 2005, pp 1837–1844.
28. Andrews, M. R.; Mitra, P. P.; de Carvalho, R. Tripling the Capacity of Wireless Communications using Electromagnetic Polarization. *Nature* 2001, **409**, pp 316–318.
29. Poon, A. S. Y.; Brodersen, R. W.; Tse, D. N. C. Degrees of Freedom in Multiple Antenna Channels: A Signal Space Approach. *IEEE Trans. Inform. Theory* 2005, **51**, pp 523–536.
30. Svantesson, T.; Jensen, M. A.; Wallace, J. W. Analysis of Electromagnetic Field Polarizations in Multiantenna Systems. *IEEE Trans. Wireless Commun.* 2004, **3**, pp 641–646.
31. Andersen, J.; Getu, B. The MIMO Cube—A Compact MIMO Antenna. *Proce. 5th Wireless Personal Multimedia Communications Int. Symp.* 2002, **1**, pp. 112–114.
32. Stancil, D. D.; Berson, A.; Hof, J. P. V.; Negi, R.; Sheth, S.; Patel, P. Doubling Wireless Capacity using Copolarized, Colocated Electric and Magnetic Dipoles. *Electron. Lett.* 2002, **38**, pp 746–747.

33. Kandonian, A. G. Three New Antenna Types and Their Applications. *Waves Electrons* 1946.

## Reading List

ITT Handbook. *Reference Data for Radio Engineers*, 5th ed.; Howard W. Sams: Indianapolis, In, 1973.

Gandhi, O. P.; Chen, J. Y. Electromagnetic Absorption in Human Head from Experimental 6-GHz Hand-Held Transceivers. *IEEE Trans. Electromagn. Compat.* 1995, **37**, pp 547–558.

Tai, C. T. On the Theory of Biconical Antennas. *J. Appl. Phys.* 1948, pp 1155–1160.

King, R. W. P. *Theory of Linear Antennas*; Harvard University Press: Cambridge, MA, 1956.

Ma, M. T.; Spies, K. P. A Simplified Formulation Computation for Conical Monopole Antennas. *U.S. Dept. of Commerce Report OT 74-53*, 1974.

Hicks, D. E. *CB Radio Antennas*; Howard W. Sams: Indianapolis, IN, 1967.

*The A.R.R.L. Antenna Book*; The American Radio Relay League: West Hartford, CT, 1956.

Johnson, R. C.; Jasik, H. *Antenna Engineering Handbook*, 2nd ed.; McGraw-Hill: New York, 1984.

Lazzi, G., et al. Comparison of FDTD-Computed and Radiation Patterns of Commercial Mobile Telephones in the Human Head. *IEEE Trans. Antennas Propagat.* 1998, **46**.

Luebbers, R., et al. FDTD Calculation of Radiation Patterns, Impedance and Gain for a Monopole Antenna on a Conducting Box. *IEEE Trans. Antennas Propagat.* 1992, **40**, pp 1577–1583.

Jensen, M. A.; Rahmat-Samii, Y. EM Interaction of Handset Antennas and a Human in Personal Communications. *Proc. IEEE* 1995, **83**, pp 7–17.

Okoniewski, M.; Stuchly, M. A. A Study of the Handset Antenna and Human Body Interaction. *IEEE Trans. Microw. Theory Tech.* 1996, **44**, pp 1855–1864.

Lazzi, G. et al. Comparison of FDTD-Computed and Radiation Patterns of Commercial Mobile Telephones in the Human Head. *IEEE Trans. Antennas Propagat.* 1998, **46**.

Gandhi, O. P.; Lazzi, G.; Furse, C. M. Electromagnetic Absorption in the Human Head and Neck for Mobile Telephones at 835 and 1900 MHz. *IEEE Trans. Microw. Theory Tech.* 1996, **44**, pp 1884–1897.

Special Issue of *IEEE Trans. Microw. Theory Tech.* 1986, MTT-34.

Durney, C. H.; Iskander, M. F. *Antenna Handbook*, Lo, Y. T., Lee, S. W. Eds.; 1993.

Sneed, P. K.; Phillips, T. L. Combining Hyperthermia and Radiation: How Beneficial? *Oncology*, 1991, **5**, pp 99–108.

Vernon, C. C.; Hand, J. W.; Field, S. B., et al. Radiotherapy With or Without Hyperthermia in the Treatment of Superficial Localized Breast Cancer: Results from Five Randomized Controlled Trials. *Int. J. Radiat. Oncol. Biol. Phys.* 1996, **35**, pp 731–744.

Turner, P. F. Interstitial Equal-Phased Arrays for EM Hyperthermia. *IEEE Trans. Microw. Theory Tech.* 1986, **34**, pp 572–578.

Furse, C. M.; Iskander, M. F. Three-Dimensional Electromagnetic Power Deposition in Tumors using Interstitial Antenna Arrays. *IEEE Trans. Biomed. Eng.* 1989, **36**, pp 977–986.

Nevels, R. D.; Arndt, G. D.; Raffoul, G. W.; Carl, J. R.; Pacifico, A. Microwave Catheter Design. *IEEE Trans. Biomed. Eng.* 1998, **45**, pp 885–890.

Manry, C.; Broschat, S. L.; Chou, C.-K.; McDougall, J. A. An Eccentrically Coated Asymmetric Antenna Applicator for Intracavity Hyperthermia Treatment of Cancer. *IEEE Trans. Biomed. Eng.* 1992, **39**, pp 935–942.

Fear, E. C.; Stuchly, M. A. Microwave Breast Tumor Detection: Antenna Design and Characterization. *IEEE Antennas Propagat. Symp. Dig.* 2000, **2**, pp 1076–1079.

Shannon, C. J.; Fear, E. C.; Okoniewski, M. Dielectric-Filled Slotline Bowtie Antenna for Breast Cancer Detection. *Electron. Lett.* 2001, **41**.

Sill, J. M.; Fear, E. C. Tissue Sensing Adaptive Radar for Breast Cancer Detection: A Study of Immersion Liquid. *Electron. Lett.* 2005, **41**, pp 113–115.

Sill, J. M.; Fear, E. C. Tissue Sensing Adaptive Radar for Breast Cancer Detection: Preliminary Experimental Results. *Proc. IEEE MTT-S Int. Microw. Symp. Dig.*; Long Beach, CA, June 2005.

Sill, J. M.; Fear, E. C. Tissue Sensing Adaptive Radar for Breast Cancer Detection—Experimental Investigation of Simple Tumor Models. *IEEE Trans. Microw. Theory Tech.* 2005, **53**, pp 3312–3319.

Wu, T.; King, R. The Cylindrical Antenna with Nonreflecting Resistive Loading. *IEEE Trans. Antennas Propagat.* 1965, **AP-13**, pp 369–373.

Wu, T.; King, R. Corrections to 'The Cylindrical Antenna with Nonreflecting Resistive Loading'. *IEEE Trans. Antennas Propagat.* 1965, **AP-13**, p 998.

Labonte, S., et al. Monopole Antennas for Microwave Catheter Absorption. *IEEE Trans. Microw. Theory Tech.* 1996, **44**, pp 1832–1840.

Wolff, E. A.. *Antenna Analysis*; Wiley: New York, 1966.

Werner, D. H. An Exact Integration Procedure for Vector Potentials of Thin Circular Loop Antennas. IEEE Trans. Antennas Propagat. 1996, **44**, pp 157–165.

Smith, G. S. Loop Antennas. In *Antenna Engineering Handbook*; McGraw-Hill: New York, 1984.

Storer, J. E. Impedance of Thin-Wire Loop Antennas. *AIEE Trans.* 1956, **75**.

Greatbatch, W.; Holmes, C. F. History of Implantable Devices. *IEEE Eng. Med. Biol.* 1991, pp 38–42.

Woolons, D. J. To Beat or Not to Beat: The History and Development of Heart Pacemakers. *IEE J. Eng. Sci. Educ.* 1995, **4**, pp 259–268.

Allan, R. Medtronic Sets the Pace with Implantable Electronics. *Electron. Design* 2003, **51**, pp 52–56.

Spelman, F. A. The Past, Present, and Future of Cochlear Prostheses. *IEEE Eng. Med. Biol.* 1999, pp 27–33.

Rauschecker, J. P.; Shannon, R. V. Sending Sound to the Brain. *Science* 2002, **295**, pp 1025–1029.

Weiland, J. D.; Humayun, M. S. A Biomimetic Retinal Stimulating Array. *IEEE Eng. Med. Biol. Mag.* 2005, **24**, pp 14–21.

Walter, P.; Kisvarday, Z. F.; Gortz, M.; Alteheld, N.; Rossler, G.; Stieglitz, T.; Eysel, U. T. Cortical Activation via an Implanted Wireless Retinal Prosthesis. *Invest. Ophthalmol. Visual Sci.* 2005, **46**, pp 1780–1785.

Margalit, E.; Maia, M.; Weiland, J. D.; Greenberg, R. J.; Fujii, G. Y.; Torres, G.; Piyathaisere, D. V.; O'Hearn, T. M.; Liu, W.; Lazzi, G.; Dagnelie, G.; Scribner, D. A.; de Juan, E.; Humayun, M. S. Retinal Prosthesis for the Blind. *Surv. Ophtalmol.* 2002, **47**, pp 335–356.

Normann, R. A.; Maynard, E. M.; Guilloty, K. S.; Warren, D. J. Cortical Implants for the Blind. *IEEE Spectrum* 1996, pp 54–59.

Zrenner, E. Will Retinal Implants Restore Vision? *Science* 2002, **295**, pp 1022–1025.

Nicolelis, M. A. L. Brain-Machine Interfaces to Restore Function and Probe Neural Circuits. *Nature Rev. Neurosci.* 2003, **4**, pp 417–422.

Chapin, J. K.; Moxon, K. A. Eds. *Neural Prostheses for Restoration of Sensory and Motor Function*. CRC Press: Boca Raton, FL, 2000.

Ghovanloo, M.; Lazzi, G. Transcutaneous Magnetic Coupling of Power and Data (invited paper). In *Wiley Encyclopedia of Biomedical Engineering*; Akay, M. Editor, Wiley (to appear, 2006).

CYNTHIA M. FURSE
OM P. GANDHI
GIANLUCA LAZZI
University of Utah
North Carolina State University